Materials Chemistry and Physics 299 (2023) 127467

Contents lists available at ScienceDirect

Materials Chemistry and Physics

journal homepage: www.elsevier.com/locate/matchemphys

Band gap engineering of anatase TiO_2 by ambipolar doping: A first principles study

S. Muthukrishnan [a,b], R. Vidya [a,b,*], Anja Olafsen Sjåstad [c]

[a] Computational Laboratory for Multifunctional Materials (CoLaMM), Department of Medical Physics, Anna University, Sardar Patel Road, Guindy, Chennai, 600025, India

[b] Centre for Materials Informatics (C-MaIn), Sir. C.V. Raman Science Block, Anna University, Sardar Patel Road, Guindy, Chennai, 600 025, India

[c] Centre Materials Science and Nanotechnology, Department of Chemistry, University of Oslo, P.O. Box: 1033, Blindern, N-0315, Oslo, Norway

HIGHLIGHTS

- Engineering the band gap and by co-doping with Sc and V impurities in TiO_2.
- Calculation of defect energetics and bonding characteristics by the impurities on anatase TiO_2.
- Exploring the effect of Jahn-Teller distortion by mono-doping and co-doping in Anatase TiO_2.
- Enhanced optical absorption in the visible region of the solar spectrum.

GRAPHICAL ABSTRACT

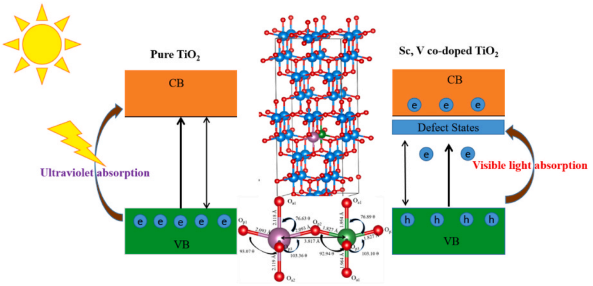

ARTICLE INFO

Keywords:
Anatase TiO_2
Ambipolar doping
Density functional theory
Band gap reduction
Visible-light absorption

ABSTRACT

Pure Anatase TiO_2 is limited to photocatalytic activity only in the UV region of solar energy, (i.e $E_g = 3.2$ eV *and* $\lambda = < 388$ nm), which utilizes only 5% of the solar spectrum. Adding external impurities to Anatase TiO_2 facilitates absorption of the visible spectrum by reducing the band gap of TiO_2. Hence, we investigated the effect of Sc and V mono-doping and co-doping on the pure anatase TiO_2 by Density Functional Theory (DFT). To elucidate the effect of doping on the electronic structure, the accurate band structure and density of states are derived using the hybrid functional methodology (HSE06). The defect formation energy of the dopants in their different charge states is calculated using the gradient-corrected density functionals using the PBE method. The bonding characteristics were analyzed using the charge density and electron-localization function (ELF) plots, which indicate that the impurities cause a local lattice distortion, which further influences the band features of TiO_2. It is observed that the formation of additional energy states by the external impurities below the conduction band minimum, reduces the band gap of the material significantly. The optical absorption analysis shows that Sc and V co-doping not only improves the absorption in the UV region, but also reaches redshift absorption. Hence the ambipolar co-doping by Sc and V to the pure anatase TiO_2 makes it a better for visible light active photocatalyst.

---

* Corresponding author. Centre for Materials Informatics (C-MaIn), Sir. C.V. Raman Science Block, Anna University, Sardar Patel Road, Guindy, Chennai, 600 025, India.

E-mail addresses: vidyar@annauniv.edu, vidyapl.ravi@gmail.com (R. Vidya).

https://doi.org/10.1016/j.matchemphys.2023.127467
Received 15 November 2022; Received in revised form 19 January 2023; Accepted 2 February 2023
Available online 3 February 2023

1. Introduction

TiO_2 is considered as the most promising semiconductor material, with enormous applications in the field of photo catalysts for pollution reduction, sensors, solar cell, water splitting, hydrogen production, and adsorption of the harmful organic molecules [1]. Naturally occurring TiO_2 exists in three polymorphs known as Anatase, Rutile and Brookite [2], with a bandgap (E_g) value of 3.2, 3.02, and 3.3 eV, respectively [3]. In 1972, Fujishima and Honda found that photo electrochemical splitting of water (H_2O into H_2 and O_2) can be achieved by irradiating the TiO_2 surface with UV light [4]. Due to the large bandgap of TiO_2, it can be operated only in the UV region as a photo catalyst. However, to carry out the redox reaction, charge carriers must be generated in the visible region of the solar spectrum [5]. Therefore, TiO_2 is activated at a wavelength of 388 nm (corresponding to the bandgap <3.2 eV) for redox reaction, which is only a small fraction of the entire solar spectrum [6]. TiO_2 can be made more functional in absorbing visible light by doping other elements to them [7]. In order to achieve the visible light-driven photo catalysts, the following conditions are necessary, (i) reducing the bandgap energy less than 3 eV, (ii) making appropriate potentials for CB and VB edges, and (iii) increasing the mobility of electron and hole charge carriers [8]. Doping the TiO_2 modifies its bandgap value by increasing the charge carriers' separation and induces more light absorption in the visible region [9]. N-doped TiO_2 shows red-shifted absorption toward the visible light, because defect states are induced above the valence band maximum by the dopant atoms [10]. The reason behind the visible light absorption of TiO_2 may be due to the bandgap narrowing and reduction in the recombination rate of electron and hole charge carriers [11]. The key mechanism which enhances the photocatalyticic activity is the formation of additional energy levels by the dopants inside the bandgap [12]. The formation of defect energy level not only enhances the absorption of photons in the UV region but also in the visible region [13].

The formation of additional energy levels in the forbidden gap may act as an electron trap, which eventually reduces the recombination of electron and hole pairs [14]. Reducing the charge carrier recombination rate is the vital step for increasing the photocatalytic activity [15]. Co-doping methods enhance the photocatalytic activity by overcoming the draw backs of mono doping, where defect level may act as the trap sites for charge carriers. Xiong et al. studied the Sc and S co-doped anatase TiO_2, and found that the synergic effect induced by co-doping increases light absorption towards the visible region [16,17]. To maintain the charge neutrality, ambipolar doping is considered. Lin et al. studied anatase TiO_2 by first principles theory, and they found that co-doping with N and Si, decreases the bandgap to 3.01 eV. The optical absorption is also improved by widening the valence band to 5.3 eV because of the Si 3p orbitals [18]. Yanming et al. studied the optical properties of C and B co-doped anatase and rutile TiO_2, by density functional theory. The generation of additional energy states reduces its bandgap by 0.8 eV, which leads to red shift optical absorption on TiO_2. Co-doping generates the hybridized energy states at the bandgap by the mixing of 2p orbitals of C and B atoms. They also found that the visible light absorption is improved by increasing the C and B concentration in TiO_2 [19]. Khan et al. studied the W and Ag co-doped anatase TiO_2 through first principle study. They found that W and Ag co-doping improves the separation of photo generated charge carriers, and reduces its bandgap. Consequently the photocatalytic visible light absorbance was improved compared to the pure TiO_2 [20]. Xuechao et al. studied the electronic and optical properties of Cr and C co-doped anatase TiO_2. The lattice distortion caused by the co-doping makes a local internal electric field, thereby enhancing the separation of the photo excited electron and hole charge carriers. It is interesting to note that, Cr and C co-doping not only reduces the bandgap, but also inhibits the recombination of electron and hole charge carriers [21]. Cristiana et al. studied the Cr and Sb co-doped TiO_2. In addition to Cr doping, an oxygen vacancy is required to induce Cr3+ state for electron transfer. By making Cr and Sb co-doping, Sb donates one electron to the Cr impurity atoms without the need Oxygen vacancies [22]. The excess charges generated by the dopants can be compensated by co-doping. Kulbir et al. studied the charge compensated Nb and Rh co-doped rutile TiO_2, where the creation of oxygen vacancy is not necessary for charge compensation [23].

One of the aims of the current study is to enhance the visible-light absorption of anatase TiO_2 by reducing its band-gap by doping. Even though the band-gap is reduced by doping with different impurity elements, the defect levels introduced by them sometimes act as recombination centres. In order to ensure charge neutrality, co-doping with simultaneous electron-donor and electron-acceptor impurities was also attempted. However, the variation in the atomic size of the co-doped elements leads to lattice distortion which may influence the behaviour of the host system under irradiation. Such lattice distortion may be minimized by introducing co-dopants of similar ionic radii. Therefore, we have taken the neighbors of Ti, viz Sc and V that have somewhat similar ionic radii like Ti for modelling the co-doping effect. By adding Sc^{3+} and V^{5+} to pure TiO_2, the excess charges of the material can be compensated. Hence the overall charges present in the structure remain neutral, consequently satisfying the valence demands. Murzin et al. successfully synthesised rutile TiO_2 with co-doping of Sc and V, and studied its structural and electrical properties [24].

2. Computational details

The simulation work based on Density Functional Theory was carried out by Plane-wave based pseudopotential method as implemented in Vienna Abinitio Simulation Package (VASP) for the self-consistent field total energy calculation [25,26]. The projected augmented wave method (PAW) exchange-correlation functional was followed. Perdew, Burke and Ernzerhof (PBE) Pseudopotentials were used to treat the core, and valence electron interaction [27]. The electron wave function was expanded by the plane wave basis set with a kinetic energy cut-off of 500 eV. A 2 × 2 x 2, and 4 × 4 x 4 k-point mesh were used for the Brillouin zone integration, for structure relaxation and electronic structure calculations respectively. The energy convergence was reached with setting the threshold value as 10^{-6} eV/atom, and the ions in the supercell were relaxed until forces on each atom less than 1 meV/Å by using conjugate gradient algorithm. A 2 × 2 x 2 supercell of 96 atoms of the TiO_2 anatase phase was considered for the GGA-PBE based calculations. For obtaining the band gap value and band dispersion accurately, Hybrid-DFT (HSE06 functional) was used [28]. A 2 × 2 x 1 supercell of 48 atoms of TiO_2 anatase phase was considered for the HSE06 based calculations. For the visualization of the crystal structure VESTA [29]packages was used. VASPKIT was used as the post-processing tool for VASP code [30].

3. Results and discussion

3.1. Geometrical optimization

The addition of external impurities to the pure TiO_2 leads to structural distortions in the lattice, which eventually influences its electronic, photocatalytic and optical properties [31]. The geometrical distortions are reflected by changes in the local coordination of the atom and the variations in bond length [32]. The relaxed geometry and its distortion of Ti–O, Sc–O, and V–O coordination are shown in Fig. 2, and the lattice parameters and atomic position are given in Table 1. The lattice parameters for pure anatase TiO_2 was obtained after the complete structural relaxation *as* $a = 3.81$ Å, $b = 3.81$ Å *and* $c = 9.70$ Å are in good agreement with the previously studied experimental [33], and the theoretical values [34]. Ti atom in pure anatase TiO_2 os coordinated to six O atoms surrounding it. Thus formed Ti–O_6 octahedra has four equivalent planar Ti–O (1.95 Å) bonds and two axial Ti–O bonds (2.00 Å). As seen from Fig. 2 (a), the axial O–Ti–O bonds almost form 180° bond angle, whereas the planar O–Ti–O bonds are bent significantly,

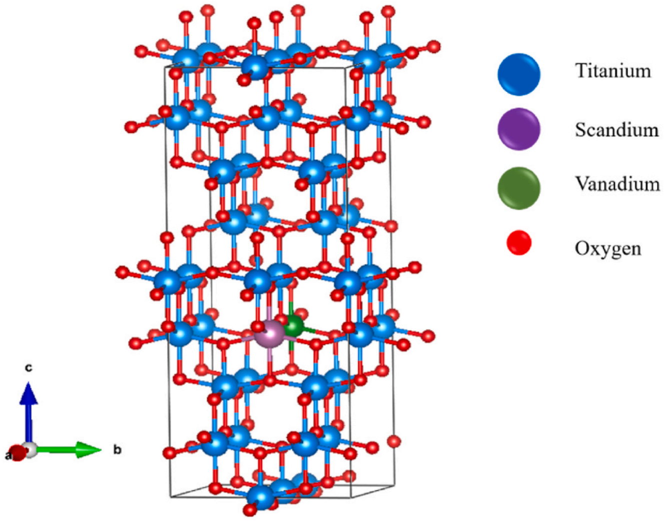

Fig. 1. The relaxed structure of 2 × 2 x 2 supercell of Sc and V co-doped anatase TiO_2. The Sc, V, Ti, and O atoms are highlighted by purple, green, blue, and red respectively. (For interpretation of the references to colour in this figure legend, the reader is referred to the Web version of this article.)

affecting the electronic structure of TiO_2.

The incorporation of Sc atom on the Ti site leads increase in bond length due to the elongation of bond, thus Sc–O coordination has the bond length of 2.04 Å and 2.15 Å, in its planer and axial bonds, respectively. Sc doping leads to the distortion of planar oxygen atoms O_{p1} and O_{p2} (Fig. 2(b)) in upward direction, the angle between the planar and axial oxygen atoms in top and bottom are 75.60° and 104.39° respectively, and the angle between the planar oxygen atoms is 93.54°. The addition of V atom on the Ti site leads to the contraction in bond length, the V–O coordination has the bond length of 1.92 Å and 1.93 Å, in its planer and axial bonds respectively. V doping leads to the distortion of planer oxygen atom atoms O_{p1} and O_{p2} (Fig. 2(c)) in downward direction, the angle between the planar and axial oxygen atoms in top and bottom are 78.44° and 101.55° respectively, and the angle between the planar oxygen atoms is 92.29°.

For the case of Sc and V co-doped structure, the bond length in Sc–O coordination is elongated and the V–O coordination is contracted, and for the Ti–O coordination the bond length is similar to the pure TiO_2. In the co-doped system, the planar and axial bond lengths are 2.09 Å, 2.11 Å and 1.82 Å, 1.95 Å for Sc–O and V–O bonds respectively. For the co-doped system, in the Sc–O coordination, the angle between the planar and axial oxygen atoms are 76.63°, and 103.36° in top and bottom respectively, the angle between the planar oxygen atoms are 93.07°. For the case of V–O coordination in the co-doped system, the angle between the planar and axial oxygen atoms are 76.89°, and 103.10° in top and bottom respectively, the angle between the planar oxygen atoms are 92.94°. The atomic radius for Sc is 160 p.m. which is higher than Ti (140 p.m.), hence Sc doping increases the cell volume to 1%. The atomic radius for V is 135 p.m., and hence the cell volume is get decreased to 1% by V doping. Similarly, the co-doping of both Sc and V increases its volume by 1%. After the co-doping, the symmetry of the structure was changed from tetragonal P-4m2 to orthorhombic Pmm2 space group, our study agrees well with the previous study done by Xiong et al. [35]. Table 1 gives the detailed geometrical structure of the system.

3.2. *Defect formation energy*

The defect formation energy is calculated in order to find the stability of the host compound after introducing the intrinsic and extrinsic defects. The defect formation energy can be calculated by the following formula,

$$\Delta H^{def}(q) = E_{tot}^{def} - E_{tot}^{bulk} \pm \sum_i n_i \mu_i q[E_V + E_F] \tag{1}$$

Where E_{tot}^{def} and E_{tot}^{bulk} denotes the total energy of doped and pure supercell respectively, E_F and E_V are the fermi energy and valence band maximum respectively, n_i indicates the total number of atoms and q is the charge state, μ_i is the chemical potential of the defect species [36]. The chemical potential of the constituent species such as Sc, Ti, and V were calculated from the formation energy of metallic Sc (hcp), Ti (hcp), and V (bcc), respectively.

The calculated defect formation energy for Sc-doped, V-doped and Sc

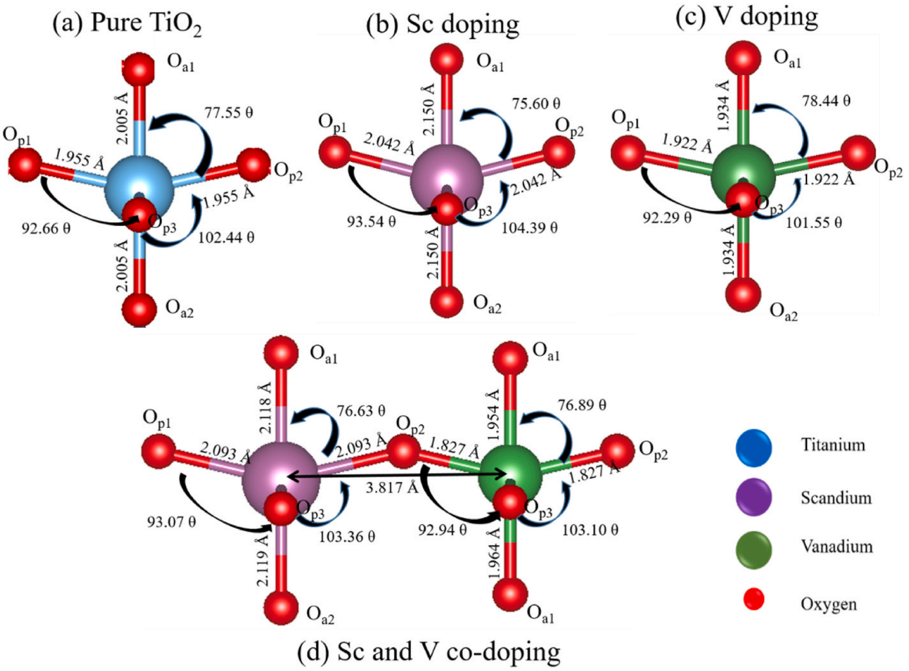

Fig. 2. Geometrical distortion of Ti–O coordination, Sc–O coordination, V–O coordination and Sc and V co-doping.

Table 1
The calculated lattice parameters, cell volume, and bond length for mono doped, and co-doped systems.

Composition	Lattice parameters (Å)				Calculated bond length (Å) and Angle (θ)					
					Ti–O		Sc–O		V–O	
	a	b	c	V	Planar	Axial	Planar	Axial	Planar	Axial
Pure	3.819	3.819	9.708	141.58	1.955 92.66°	2.005 102.44°	–	–	–	–
Sc -doped	3.827	3.827	9.717	142.31 (1%)	1.974 1.906 93.34°	2.045 2.060 104.04°	2.042 93.54°	2.150 104.39° 75.60°	–	–
V –doped	3.819	3.819	9.690	141.32 (−1%)	1.954 1.977 92.40°	1.993 1.996 101.75°	–	–	1.922 92.29°	1.934 101.55° 78.44°
Sc & V codoped	3.817	3.820	9.741	142.03 (1%)	1.953 1.989 1.928 93.33°	1.980 2.031 101.27° 78.59°	2.024 2.093 93.07°	2.118 2.119 103.36° 76.63°	1.827 1.902 92.94°	1.954 1.964 103.10° 76.89°

and V co-doped TiO_2 with various charge defects as a function of Fermi energy is shown in Fig. 3. “The configuration energy defined as the difference in the total energy of the supercell with defects and that of the pure supercell, gives an idea about the stability of system after introducing defects. The calculated configuration energy obtained from the optimized total energies was a negative value for Sc in 3+ charge state (−0.0841 eV) and V in 2+ (−0.4775 eV) and 3+ (−0.9584 eV) charge states. This implies that the anatase TiO_2 remains stable when Sc and V are introduced as defects into the TiO_2 lattice.”

The formation energy at zero charge states for Sc doped, V doped, and Sc and V co-doped TiO_2 is 1.079 eV, 2.404 eV, and 1.466 eV, respectively. This implied that Sc doping is energetically favourable. But, the formation energy of Sc–V co-doped TiO_2 is less than that of V doped TiO_2. Hence the Sc doping not only favours charge compensation, but also improves the stability of the co-doped system, which agrees with the experimental observation of similar co-doping done by Murzin et al. [24].

3.3. Electronic structure analysis

The projected density of states (PDOS) for pure anatase TiO_2 is shown in Fig. 4(a). From the hybrid functional calculations, the calculated band gap of pure anatase TiO_2 is about 3.48 eV which is in good agreement with the previous study [37], whereas the experimental bandgap is about 3.2 eV [38]. From the PDOS analysis, it is seen that the valence band is contributed by the O-2p orbitals and the conduction band is mainly contributed by the Ti-3d orbitals.

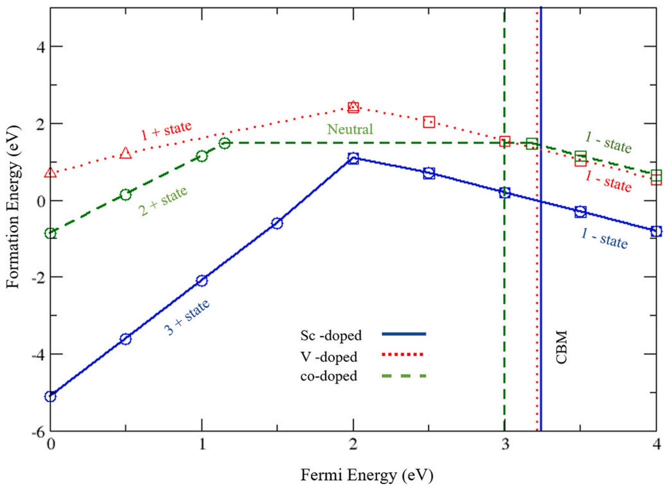

Fig. 3. Calculated defect formation energy with GGA-PBE functionals, for Sc doped, V doped, and Sc, V co-doped TiO_2 at different charge (q) states with respect to the Fermi Energy (E_F).

Usually Sc has the valence state of 3+, whereas Ti has 4+ valence state. The DOS analysis shows that the Sc doping at the Ti site leads to reduction in the band gap by about 0.24 eV. From the PDOS given in Fig. 4(b), no impurity state contributed by Sc is seen in the forbidden gap. The Sc dopant is supposed to introduce acceptor energy levels close to VBM. This is consistent with the small extra peak of PDOS seen at the E_F (Fig. 4(b)), having the width of about 0.3 eV and mainly made of O-2p orbitals. Sc doping increase in the hole mobile charge carriers which is reflected by the shifting of fermi energy level towards the valence band maximum (VBM).

Generally, V can take up the oxidation states 2+, 3+, 4+ and 5+ in oxides. The PDOS of V-doped TiO_2 is given in Fig. 4(c). It can be seen that the band gap of TiO_2 is reduced by ~0.26 eV due to V doping. Moreover, the E_F moves towards the CBM, and a few additional states appear close to the CBM (0–0.5eV). The Ti-d and V-d states are degenerate in this energy region.

To understand the effect of ambipolar doping of Sc and V into TiO_2, the plots of PDOS of Sc, V co-doped anatase TiO_2 is shown in Fig. 4(d). Unlike the V-doped case, the E_F lies close to VBM in the co-doped system. Interestingly additional states are seen close to the CBM in the energy range of 3–3.5 eV. This isolated DOS region is mainly contributed by V-3d orbitals.

The effect of Sc and V doping on the band features of TiO_2 is schematically shown in Fig. 5. The addition of Sc in co-doping drives the separation of V-3d states that are close to CBM, which reduces the bandgap of TiO_2 from 3.48 eV to 3.0 eV. The band gap obtained for the pure system is 3.48 eV (from hybrid functional calculations) which is over estimated by 0.28 eV than the experimental band gap value (3.2 eV). By including the scissor operation, the band gap value obtained for Sc and V doping are 2.96 eV, and 2.94 eV, respectively, after correcting the over-estimation error. Similarly, a band-gap value of 2.72 eV was obtained for the Sc–V co-doped TiO_2. Thus Sc and V co-doped TiO_2 absorb more visible light, and thus can eventually enhance the photocatalytic activity in the visible region.

3.4. Chemical bonding analysis

To understand the nature of chemical bonding of the mono doped and co-doped system, the charge density (Fig. 6) and the Electron localization function (Fig. 7) analysis were carried out. The contour plots of the electron localization function along the 001 plane for pure, Sc doped, V doped, and Sc, V co-doped anatase TiO_2, is shown in Fig. 7. Even though the electronegativity difference between Ti and O is 1.9, Ti–O bond has significant covalent characteristics in addition to the ionic nature. This is consistent with the previous study by C Sousa et al. [39]. The local structure of TiO_2 is disturbed by Sc doping. It is interesting to note that Sc–O bonds show more covalent character even

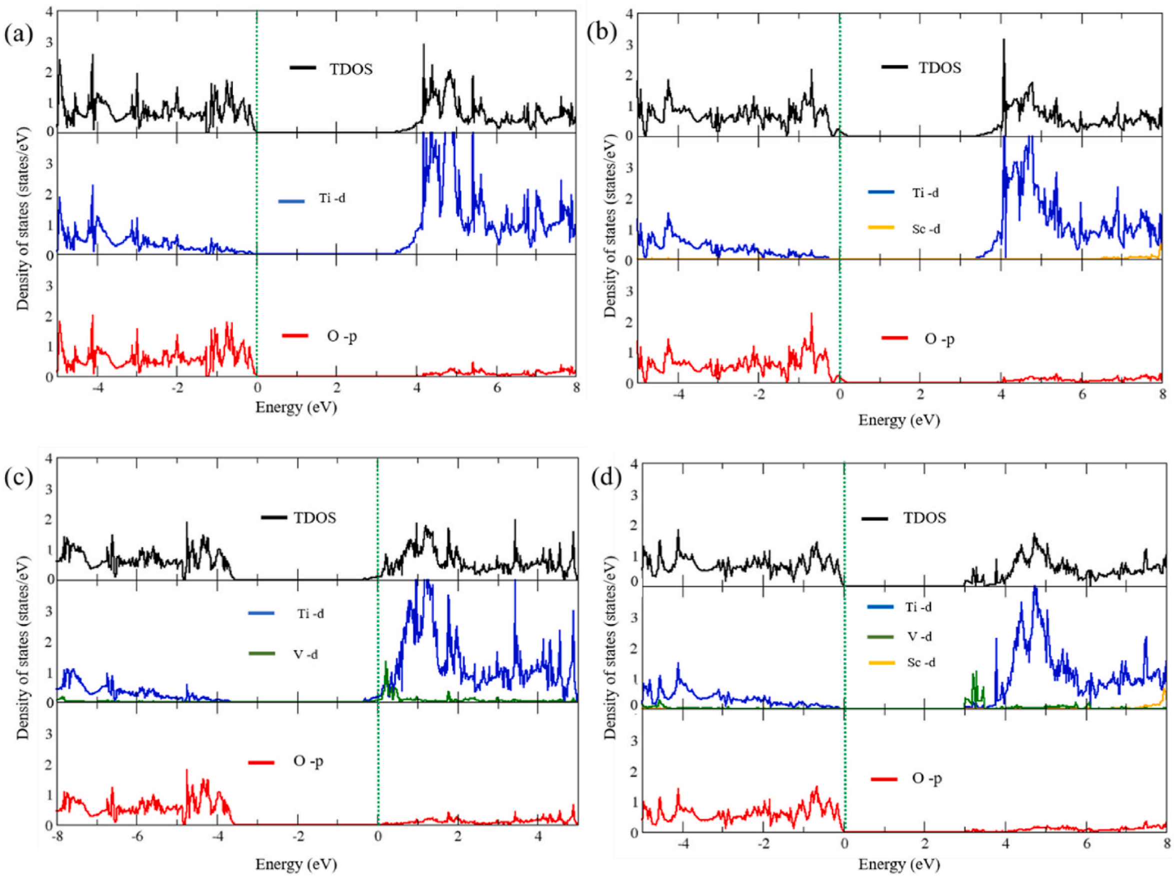

Fig. 4. Projected Density of states plots for (a) pure, (b) Sc doped, (c) V doped, and (d) Sc, V co-doped anatase TiO_2. The fermi level is shifted to 0 eV, indicated by vertical dotted green lines. (For interpretation of the references to colour in this figure legend, the reader is referred to the Web version of this article.)

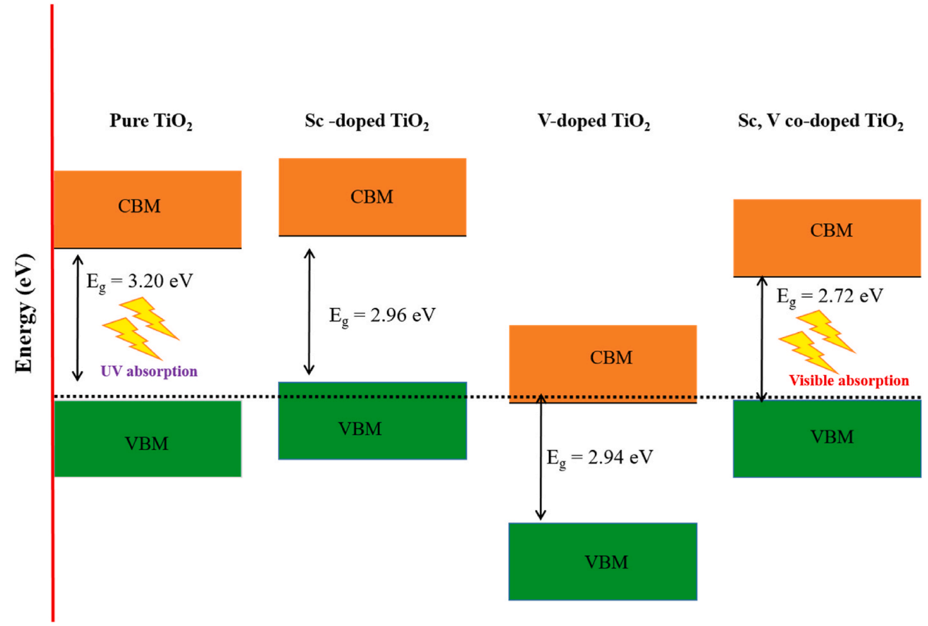

Fig. 5. The schematic representation for band edge positions for pure, monodoped, and co-doped anatase TiO_2. The fermi level is shifted to 0 eV.

though the electronegativity difference is 2.08 (higher than that of pristine Ti–O). However, the nature of ionic bonding is also non-negligible. Owing to the presence of Sc, the lattice is locally distorted in which the Ti–O bonds undergoing significant changes. The basal Ti–O bonds exhibit more covalent character and the Sc–O bond lengths are elongated compared to the Ti–O bonds (observed from the charge density and ELF plots in Figs. 6 and 7).

Since the electronegativity bonds between V–O is smaller (1.81) than

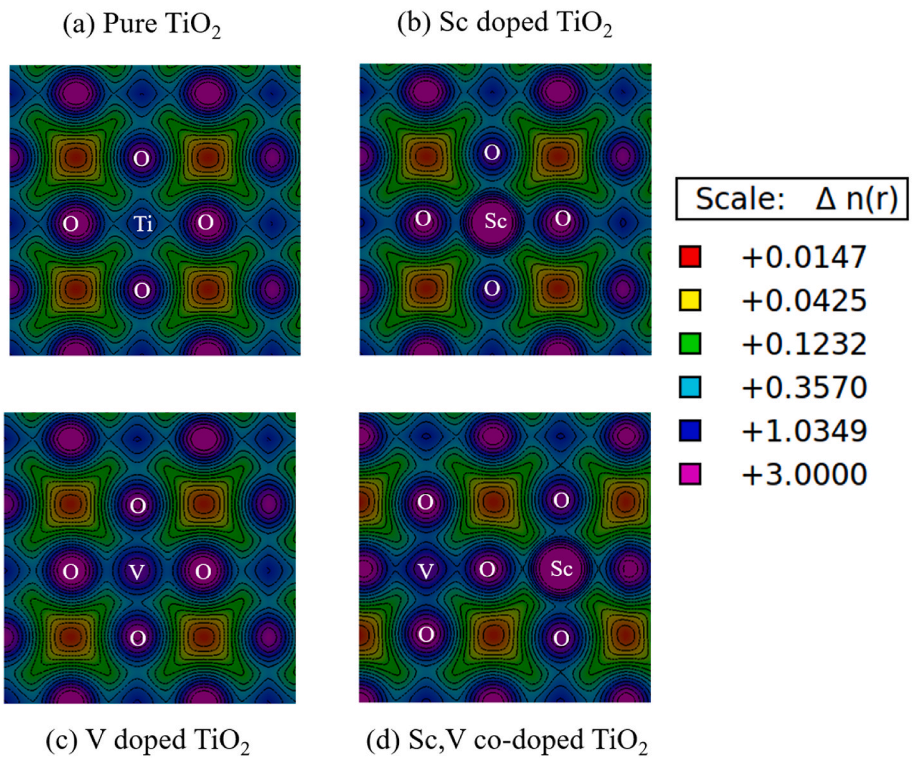
(a) Pure TiO_2
(b) Sc doped TiO_2
(c) V doped TiO_2
(d) Sc,V co-doped TiO_2

Fig. 6. The Charge density for pure (a), Sc –doped (b), V –doped (c), and Sc, V codoped (d) anatase TiO_2 along (001) plane.

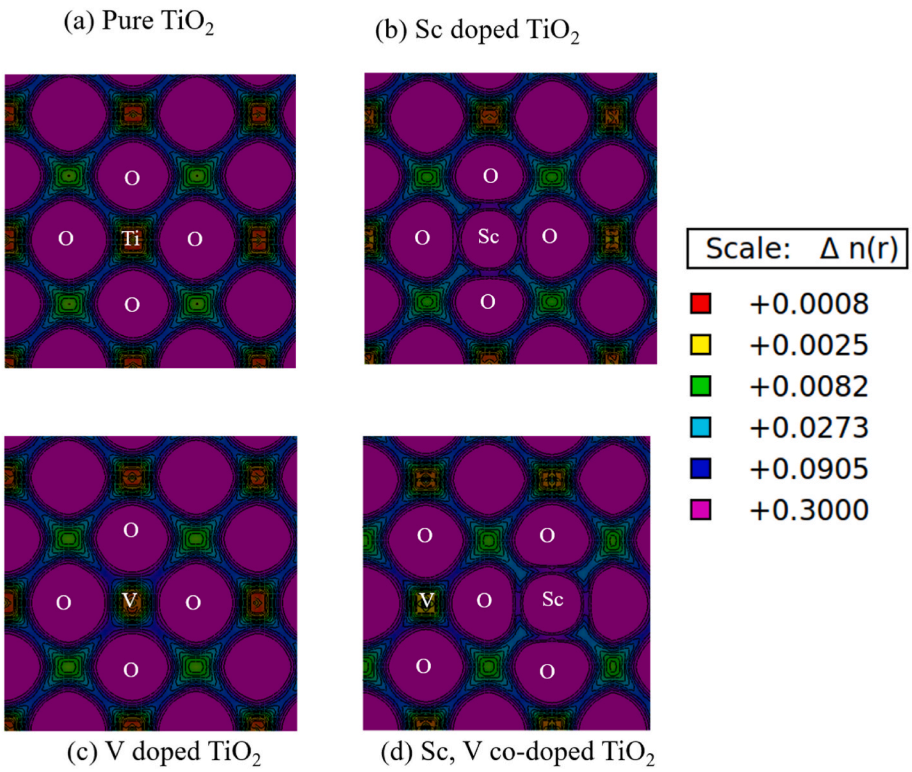
(a) Pure TiO_2
(b) Sc doped TiO_2
(c) V doped TiO_2
(d) Sc, V co-doped TiO_2

Fig. 7. The Electron localization function for pure (a), Sc –doped (b), V –doped (c), and Sc, V codoped (d) anatase TiO_2 along (001) plane.

that of Ti–O (1.9). The V–O bonds are expected to be more predominantly covalent. More numbers of contours seen between the charge density and ELF plots (Figs. 6 and 7) are consistent with the following assumption. The significant reduction in the V–O bond length (seen along the basal as well as axial planes) compared to the Ti–O bonds, could be resulting because of the stronger V–O covalent bonds. It is interesting to analyze the effect of ambipolar doping (V as donor and Sc as acceptor) in TiO_2. The elongation in the Sc–O bond length and the contraction in the V–O bond length seen in the monodoping are also maintained in the co-doping case of TiO_2.

3.5. Optical properties analysis

The optical properties of the materials are calculated from the frequency dependent complex dielectric function which consists of real [$\varepsilon_1(\omega)$] and the imaginary [$\varepsilon_2(\omega)$] parts, as stated by the following equation,

$$\varepsilon(\omega) = \varepsilon_1(\omega) + i\varepsilon_2(\omega) \tag{2}$$

The real and imaginary part of the dielectric function shows the capacity of light reflection and absorption of the material respectively [40]. The imaginary [$\varepsilon_2(\omega)$] part is calculated from summing over the empty bands, and the real part [$\varepsilon_1(\omega)$] is obtained by Kramers-Kronig transformations [$\varepsilon_2(\omega)$] [41,42]. The absorption coefficient is calculated from the following equation [43],

$$\alpha(\omega) = \left[2\left[\sqrt{\varepsilon_1^2(\omega) + \varepsilon_2^2(\omega)} - \varepsilon_1(\omega)\right]\right]^{1/2} \tag{3}$$

Fig. 8 (a) shows the absorption coefficient of the pure TiO_2, Sc doped TiO_2, V doped TiO_2, and Sc, V co-doped TiO_2, which is calculated from equation (3). It can be seen that, the absorption coefficient of pure TiO_2, and the Sc doped TiO_2 is almost similar. The absorption starts from 2.5 eV, corresponding to the UV region. Since V doping introduces electron charge carriers, which brings in metal like nature (Fig. 4(c)), a broad absorption peak is seen at the IR region. Sc and V co-doping leads to improvement in the optical absorption coefficient (Fig. 8(a)). The insert in Fig. 8(a) clearly shows that, the optical absorption starts from 2 eV in the co-doped system. The co-doped system achieves red-shift absorption compared to the pure and mono doped systems. The optical absorption plots of the pure, mono doped, and co-doped system replicates the band structure plots of all the TiO_2 systems, where the band gap is considerably reduced (given in Fig. 1 of the Supplementary Information). Due to Sc and V charge compensated co-doping, the additional energy states formed at the CBM, decreases the electronic transition energy, which eventually improves the light absorption towards the visible light. Fig. 8 (b) shows the imaginary part of dielectric constant as a function of energy. In the energy range from 2.5 eV to 3.5 eV, the pure, mono doped, and co-doped TiO_2 has two absorption peaks at 2.8 eV and 3.4 eV, respectively. From 2 eV the co-doped system shows enhanced optical absorption, compared to mono doped and pure TiO_2. From the optical spectra, we can ensure that, the Sc, V co-doped TiO_2 increases the absorption and also expands the light absorption edge towards the visible region.

4. Conclusion

The structural, electronic, and optical properties of the anatase TiO_2, which is mono doped with Sc and V, and their co-doping are studied by Density Functional Theory. It may be noted that V-doping in V^{5+} charge state becomes a donor, whereas Sc-doping in Sc^{3+} state becomes an acceptor, resulting in charge compensation in the co-doped TiO_2. In addition, this ambipolar impurity combination induces a large local structural distortion in the form of Jahn-Teller distortion, resulting in enhanced stability for the co-doped system. The formation energy for Sc_{Ti} and V_{Ti} in various charge states is calculated as a function of fermi energy. To obtain the bandgap of pure and doped systems accurately, the hybrid functional calculation (HSE06) was used. The band gap obtained for the pure system is 3.48 eV which is over-estimated by 0.28 eV than the experimental band gap value (3.2 eV). From the scissor operator, the band gap value obtained for Sc and V doping are 2.96 eV and 2.94 eV respectively, after including the over-estimation error. Similarly, a band-gap value of 2.72 eV was obtained for the Sc–V co-doped TiO_2. The reduction in the band-gap is resulting due to the additional energy states, formed below the conduction band minimum. This implies that Sc–V co-doping can lead to the absorption in visible energy range, which will further enhance the photo-conversion efficiency of TiO_2.

The excited-state properties like optical absorption and dielectric tensor are calculated for the pure and doped systems. It is found that, the Sc and V co-doping shifts the optical absorption from 2.5 eV to 2.0 eV, which corresponds to the visible region. The bonding characteristics were studied by the electronic charge density and the electron localization function analyses. The V–O bonds are expected to be more predominantly covalent. The Sc–O bonding shows more ionic nature than Ti–O bonding. The elongation in the Sc–O bond and the contraction in the V–O bond seen in the monodoping are maintained in the co-doping case also. Overall we have studied the electronic structure by the effect of Sc/V doping and co-doping on the anatase TiO_2. We found that, Sc/V co-doping can lead to local structural distortion, and enhancement the optical absorption in the visible region.

CRediT authorship contribution statement

S. Muthukrishnan: Data curation, Formal analysis, Writing – original draft, collecting the data, performed the analysis, wrote the paper. **R. Vidya:** Data curation, Formal analysis, Writing – original draft, collecting the data, performed the analysis, wrote the paper. **Anja Olafsen Sjåstad:** Formal analysis, Conceptualization, designed the analysis.

Declaration of competing interest

The authors declare the following financial interests/personal relationships which may be considered as potential competing interests: Dr R Vidya reports financial support was provided by Anna University.

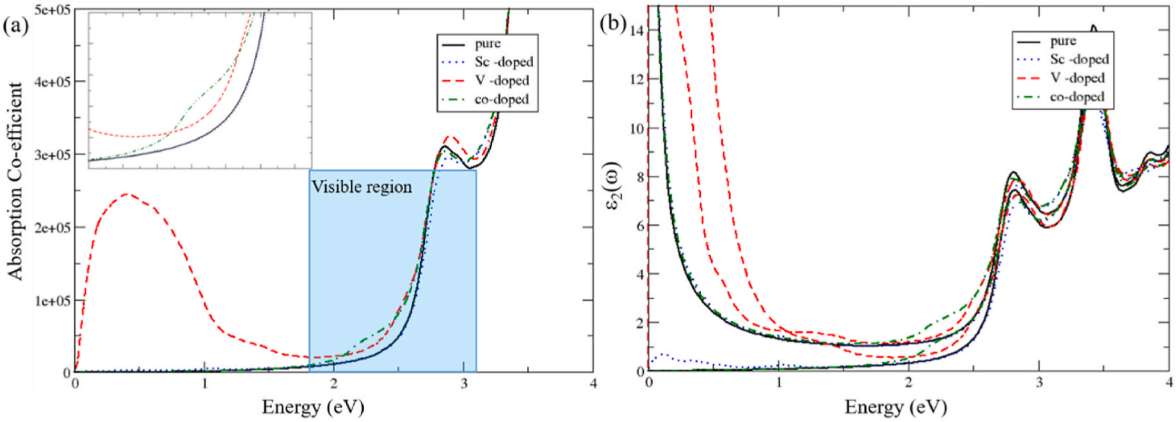

Fig. 8. (a) The absorption coefficient of pure, mono doped, and co-doped TiO_2, the insert indicates shift in optical absorption, (b) the imaginary part of dielectric constant for pure, mono doped, and co-doped TiO_2, as a function of Energy.

Dr Anja Olafsen Sjastad reports financial support was provided by University of Oslo.

Data availability

Data will be made available on request.

Acknowledgments

The authors acknowledge University of Oslo, Norway for providing the financial support through Indo-Norway project (CIR/60/INDO-NORWAY/2019). The authors are grateful to the Norwegian supercomputer facilities (Project No: NN2875K) for computing time.

Appendix A. Supplementary data

Supplementary data to this article can be found online at https://doi.org/10.1016/j.matchemphys.2023.127467.

References

[1] K. Nakata, A. Fujishima, TiO 2 photocatalysis: design and applications, J. Photochem. Photobiol. C Photochem. Rev. 13 (3) (2012) 169–189, https://doi.org/10.1016/j.jphotochemrev.2012.06.001.

[2] M. Zhang, T. Chen, Y. Wang, Insights into TiO2 polymorphs: highly selective synthesis, phase transition, and their polymorph-dependent properties, RSC Adv. 7 (83) (2017) 52755–52761, https://doi.org/10.1039/c7ra11515f.

[3] U. Diebold, Structure and properties of TiO2 surfaces: a brief review, Appl. Phys. Mater. Sci. Process 76 (5) (2003) 681–687, https://doi.org/10.1007/s00339-002-2004-5.

[4] Fijishima, et al., Electrochemical photolysis of water at a semiconductor electrode, Nature 238 (5358) (1972) 37–38.

[5] A. Truppi, et al., Visible-light-active TiO2-based hybrid nanocatalysts for environmental applications, Catalysts 7 (2017), https://doi.org/10.3390/catal7040100, 4.

[6] W. Ren, Z. Ai, F. Jia, L. Zhang, X. Fan, Z. Zou, Low temperature preparation and visible light photocatalytic activity of mesoporous carbon-doped crystalline TiO2, Appl. Catal. B Environ. 69 (3–4) (2007) 138–144, https://doi.org/10.1016/j.apcatb.2006.06.015.

[7] H. Wang, J.P. Lewis, Effects of dopant states on photoactivity in carbon-doped TiO2, J. Phys. Condens. Matter 17 (2005), https://doi.org/10.1088/0953-8984/17/21/L01, 21.

[8] L. Zhang, et al., Photo degradation of methyl orange by attapulgite-SnO2-TiO2 nanocomposites, J. Hazard Mater. 171 (1–3) (2009) 294–300, https://doi.org/10.1016/j.jhazmat.2009.05.140.

[9] S.B. Yang, H.H. Chun, R.J. Tayade, W.K. Jo, Iron-functionalized titanium dioxide on flexible glass fibers for photocatalysis of benzene, toluene, ethylbenzene, and o-xylene (BTEX) under visible- or ultraviolet-light irradiation, J. Air Waste Manag. Assoc. 65 (3) (2015) 365–373, https://doi.org/10.1080/10962247.2014.995838.

[10] A.V. Emeline, V.N. Kuznetsov, V.K. Rybchuk, N. Serpone, Visible-light-active titania photocatalysts: the case of N-doped TiO2 s—properties and some fundamental issues, Int. J. Photoenergy (2008) 1–19, https://doi.org/10.1155/2008/258394, 2008.

[11] J. Ouyang, M. Chang, X. Li, CdS-sensitized ZnO nanorod arrays coated with TiO 2 layer for visible light photoelectrocatalysis, J. Mater. Sci. 47 (9) (2012) 4187–4193, https://doi.org/10.1007/s10853-012-6273-x.

[12] W. Xie, R. Li, Q. Xu, Enhanced photocatalytic activity of Se-doped TiO2 under visible light irradiation, Sci. Rep. 8 (1) (2018) 1–10, https://doi.org/10.1038/s41598-018-27135-4.

[13] R. Khan, S.W. Kim, T.J. Kim, C.M. Nam, Comparative study of the photocatalytic performance of boron-iron Co-doped and boron-doped TiO2 nanoparticles, Mater. Chem. Phys. 112 (1) (2008) 167–172, https://doi.org/10.1016/j.matchemphys.2008.05.030.

[14] R. Qian, et al., Charge carrier trapping, recombination and transfer during TiO2 photocatalysis: an overview, Catal. Today 335 (2019) 78–90, https://doi.org/10.1016/j.cattod.2018.10.053. October 2018.

[15] M. Anpo, M. Takeuchi, The design and development of highly reactive titanium oxide photocatalysts operating under visible light irradiation, J. Catal. 216 (1–2) (2003) 505–516, https://doi.org/10.1016/S0021-9517(02)00104-5.

[16] K. Xiong, Q. Zheng, Z. Cheng, P.F. Liu, Structural, electronic and optical properties of S-doped, Sc-doped and Sc–S co-doped anatase TiO2: a DFT + U calculation, Eur. Phys. J. B 93 (2020), https://doi.org/10.1140/epjb/e2020-10368-x, 11.

[17] Y. Zhao, L. He, Charge compensation co-doping enhances the photocatalytic activity of black phosphorus, Mol. Catal. 516 (2021), 112008, https://doi.org/10.1016/j.mcat.2021.112008. November.

[18] H. Lin, H. Wu, Electronic Structure and Optical Properties of N/Si-Codoped Anatase TiO 2 Evaluated Using First Principles Calculations, 2014, 2014.

[19] Yanming Lin, et al., C/B co-doping effect on Band gap narrowing and optical performance of TiO2 photocatalysts: a spin polarized DFT study, 4516, J. Mater. Chem. 1 (2013) 4516–4524, https://doi.org/10.1039/c3ta01298k, 2013.

[20] M. Khan, et al., Enhanced photoelectrochemical properties of TiO2 by codoping with tungsten and silver Enhanced photoelectrochemical properties of TiO 2 by codoping with tungsten and silver, J. Appl. Phys. 115, (2014) 153103, https://doi.org/10.1063/1.4871977.

[21] X. Li, et al., A DFT study on the modification mechanism of (Cr, C) co-doping for the electronic and optical properties of anatase TiO2, Comput. Mater. Sci. 129 (2017) 295–303, https://doi.org/10.1016/j.commatsci.2016.12.029.

[22] C. Di Valentin, G. Pacchioni, H. Onishi, A. Kudo, Cr/Sb co-doped TiO2 from first principles calculations, Chem. Phys. Lett. 469 (1–3) (2009) 166–171, https://doi.org/10.1016/j.cplett.2008.12.086.

[23] K.K. Ghuman, C.V. Singh, A DFT + U study of (Rh, Nb)-codoped rutile TiO2, J. Phys. Condens. Matter 25 (8) (2013), https://doi.org/10.1088/0953-8984/25/8/085501.

[24] P.D. Murzin, A.A. Murashkina, A.V. Emeline, D.W. Bahnemann, Effect of Sc3+/V5 + Co-doping on photocatalytic activity of TiO2, Top. Catal. 64 (13–16) (2021) 817–823, https://doi.org/10.1007/s11244-020-01292-1.

[25] G. Kresse, J. Hafner, Ab initio molecular dynamics for liquid metals, Phys. Rev. B 47 (1) (1993) 558–561, https://doi.org/10.1103/PhysRevB.47.558.

[26] D. Joubert, From ultrasoft pseudopotentials to the projector augmented-wave method, Phys. Rev. B Condens. Matter 59 (3) (1999) 1758–1775, https://doi.org/10.1103/PhysRevB.59.1758.

[27] J.P. Perdew, K. Burke, M. Ernzerhof, Generalized gradient approximation made simple, Phys. Rev. Lett. 77 (18) (1996) 3865–3868, https://doi.org/10.1103/PhysRevLett.77.3865.

[28] J. Heyd, G.E. Scuseria, M. Ernzerhof, Hybrid functionals based on a screened Coulomb potential, J. Chem. Phys. 118 (18) (2003) 8207–8215, https://doi.org/10.1063/1.1564060.

[29] K. Momma, F. Izumi, VESTA: a three-dimensional visualization system for electronic and structural analysis, J. Appl. Crystallogr. 41 (3) (2008) 653–658, https://doi.org/10.1107/S0021889808012016.

[30] V. Wang, N. Xu, J.C. Liu, G. Tang, W.T. Geng, VASPKIT: a user-friendly interface facilitating high-throughput computing and analysis using VASP code, Comput. Phys. Commun. 267 (2021), 108033, https://doi.org/10.1016/j.cpc.2021.108033.

[31] M. Nishikawa, S. Yuto, T. Nakajima, T. Tsuchiya, N. Saito, Effect of lattice distortion on photocatalytic performance of TiO2, Catal. Lett. 147 (1) (2017) 292–300, https://doi.org/10.1007/s10562-016-1928-x.

[32] Y. Hu, et al., Lattice distortion induced internal electric field in TiO2 photoelectrode for efficient charge separation and transfer, Nat. Commun. 11 (1) (2020) 1–10, https://doi.org/10.1038/s41467-020-15993-4.

[33] T. Arlt, M. Bermejo, M. Blanco, High-pressure polymorphs of anatase, Phys. Rev. B Condens. Matter 61 (21) (2000) 14414–14419, https://doi.org/10.1103/PhysRevB.61.14414.

[34] M. Arrigoni, G.K.H. Madsen, A comparative first-principles investigation on the defect chemistry of TiO2 anatase, J. Chem. Phys. 152 (4) (2020), https://doi.org/10.1063/1.5138902.

[35] K. Xiong, Q. Zheng, Z. Cheng, P. Liu, Structural , Electronic and Optical Properties of S-Doped , Sc-Doped and Sc – S Co-doped Anatase TiO 2 : a DFT + U Calculation, 2020.

[36] R. Vidya, P. Ravindran, H. Fjellvag, B.G. Svenssos, E. Monakhov, M. Ganchenkova, R.M. Nieminen, Energetics of intrinsic defects and their complexes in ZnO investigated by density functional calculations, Phys. Rev. B Condens. Matter 83 (4) (2011), https://doi.org/10.1103/PhysRevB.83.045206.

[37] J. Liu, et al., High-throughput HSE study on the doping effect in anatase TiO2, Phys. Chem. Chem. Phys. 22 (1) (2019) 39–53, https://doi.org/10.1039/c9cp04591k.

[38] C. Dette, et al., TiO2 anatase with a bandgap in the visible region, Nano Lett. 14 (11) (2014) 6533–6538, https://doi.org/10.1021/nl503131s.

[39] C. Sousa, F. Illas, Ionic-covalent transition in titanium oxides, Phys. Rev. B 50 (19) (1994) 13974–13980, https://doi.org/10.1103/PhysRevB.50.13974.

[40] R.S. Dima, L. Phuthu, N.E. Maluta, J.K. Kirui, R.R. Maphanga, Dye-Sensitized Solar Cells — A First Principles Study 210 (2021).

[41] T. Premkumar, R. Vidya, H. Fjellvåg, Stabilizing p -type conductivity in CuYO 2 by co-doping : a first-principles study, Mater. Chem. Phys. 285 (April) (2022).

[42] D. Bharath Raja, K. Shanmuga Sundaram, R. Vidya, First principle study on hybrid organic-inorganic perovskite ASnBr3 (A = Formamidinium, Dimethylammonium and Azetidinium), Sol. Energy 207 (2020) 1348–1355, https://doi.org/10.1016/j.solener.2020.07.044. July.

[43] H.X. Zhu, X.H. Wang, D.F. Zhou, H. Jiang, X.M. Liu, First-principles study on electronic, magnetic properties and optical absorption of vanadium doped rutile TiO2, Phys. Lett. Sect. A Gen. At. Solid State Phys. 384 (26) (2020), 126637, https://doi.org/10.1016/j.physleta.2020.126637.